AGU100 ADVANCING EARTH AND SPACE SCIENCE

Radio Science

RESEARCH ARTICLE

10.1029/2018RS006692

Key Points:

- Numerically computing magnetic field expressions to achieve computational accuracy and feasibility are comprised
- A method for accurately numerical evaluation of the Sommerfeld integral for subsurface applications is proposed
- Matlab implementation of the aforementioned points validated by comparative study with Finite Element Method by COMSOL simulations is provided

Correspondence to:
N. Ayuso,
nayuso@unizar.es

Citation:
Ayuso, N., Cuchí, J. A., Lera, F., & Villarroel, J. L. (2019). A computational channel model for magnetic induction-based subsurface applications. *Radio Science*, *54*, 822–838. https://doi.org/10.1029/2018RS006692

Received 26 JUL 2018
Accepted 7 JUL 2019
Accepted article online 24 JUL 2019
Published online 10 SEP 2019

A Computational Channel Model for Magnetic Induction-Based Subsurface Applications

Natalia Ayuso[1,2], José Antonio Cuchí[1,2], Francisco Lera[1,2], and José Luis Villarroel[1,2]

[1]Aragón Institute of Engineering Research (I3A), University of Zaragoza, Zaragoza, Spain, [2]Group of Technologies in Hostile Environments (GTE) University of Zaragoza, Zaragoza, Spain

Abstract There are many underground applications based on magnetic fields generated by an oscillating magnetic source. For them, a magnetic dipole in a three-layered region with upper semi-infinite air layer can be a convenient idealization used for their planning, development, and operation. Solutions are in the form of the well-known Sommerfeld integral expressions that can be evaluated by numerical methods. A set of field expressions to be numerically evaluated by an efficient algorithm are not collected comprehensively yet, or at least in a directly usable form. In this paper, the explicit magnetic field solutions for the vertical magnetic dipole and the horizontal magnetic dipole for a general source-observer location are derived from the Hertz vector. They can be properly combined to model the problem of a tilted magnetic dipole source for horizontally or inclined stratified media. As a result, a complete set of integral equations of the Sommerfeld type valid from the near zone to the far zone are formulated. A method for numerical evaluation of the field expressions for high accurate computations is described. The numerical results are validated using the finite element method for all the possible source-receiver configurations and three well-spanned frequencies of typical subsurface applications. Both numerical solutions agree according to the normalized root-mean-square error-based fit metric. Numerical results for two cases of study are presented to see its usefulness for subsurface applications. A MATLAB implementation of the mathematical description outlined in this paper and the proposed evaluation method is freely available for download.

1. Introduction

Nowadays, there is a growing interest in using magnetic induction systems for geophysics (see Abdu et al., 2007; Becker et al., 1992; Corwin & Lesch, 2003; Durkin, 1991; Heil & Schmidhalter, 2017), location (see eg. Ayuso et al., 2010; Davis et al., 2008; Markham et al., 2012; Sogade et al., 2004), emergency communications in confined environments such as mines or caves (see Bandyiopadhyay et al., 2010; Yan et al., 2013a), and wireless underground and undersea communication networks (see, e.g., Akyildiz et al., 2015; Akyildiz & Stuntebeck, 2006a; Domingo, 2014; Sun & Akyildiz, 2010; Tan et al., 2015; Wang et al., 2014).

These contemporary applications are very challenging because of the rapid decay of the received signal strength with distance, the signal distortion due to the subsurface medium or system constraints as limited autonomy and bandwidth. Therefore, optimization of the communication parameters is of paramount importance for such emerging technologies (Abrudan et al., 2016; Silva & Moghaddam, 2015; Tan et al., 2015). To this end, a channel model that accurately characterizes the complex underground environment is necessary. In many situations, the background can be more conveniently idealized as horizontally stratified media, that is, air-soil, air-soil-type$_1$, air-soil-type$_2$, air-sea-seabed, or air-snow-soil than free-space or infinite medium. Besides, a magnetic dipole approximation for a small transmitting loop is convenient for observation points located at a few loop radii. In Ayuso et al. (2006), Durkin (1991), Large et al. (1973), Yan et al. (2013b), and Wang et al. (2014), such model predictions are compared with real data with good agreement. As expected, a more complex model as Finite Element Method (FEM) used in Ayuso et al. (2009), fairly improve the predictions. However, the model definition is quite complex and computation requirements in terms of calculation time and memory requirements are especially high. In conclusion, communication channel for magnetic induction (MI)-based subsurface applications can be conveniently modeled by magnetic field expressions for a three-layered model with upper air layer, a central layer of finite depth, and lower layer of infinite extension.

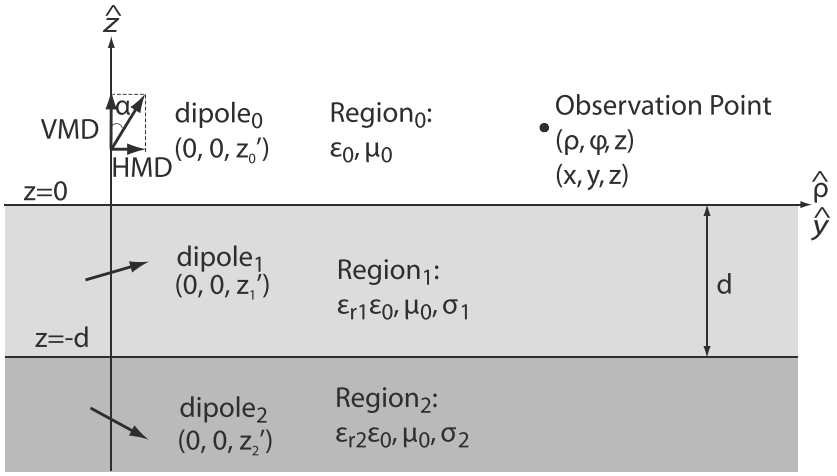

Figure 1. Three-layered medium model for calculating the magnetic fields of an arbitrarily oriented magnetic dipole. For example, Region 1 concerns moisturized soil or snow and Region 2 accounts for the underlying soil. VMD = vertical magnetic dipole; HMD = horizontal magnetic dipole.

Electromagnetic (EM) waves propagation from Hertzian dipoles in the presence of isotropic layered media has been extensively investigated since the pioneering work by Sommerfeld in 1909 (Sommerfeld, 1909, 1926) to the present time (Fei et al., 2007; Guzatov et al., 2013; Guzatov & Klimov, 2014; Liao & Sarabandi, 2007; Liu & Li, 2007; Long et al., 2001; Michalski & Mosig, 2016; Wang et al., 2014, 2015). As a result, the EM fields from a vertical magnetic dipole (VMD) or a horizontal magnetic dipole (HMD) in the presence of a two-layered or multilayered region have been presented in analytical closed-form expressions by many researchers, in particular, by Wait (1961, 1996, 1969, 1972, 1982). However, because the solutions are expressed in terms of the Sommerfeld integrals, approximated formulae have been extensively derived due to the intricacy of evaluating their oscillating infinite nature. Therefore, the range of validity of these expressions has been normally limited to the near or far region (see, e.g., Inan & Fraser-Smith, 1990; Layman, 1981; Long et al., 2001; Sinha & Bhattacharya, 1966). Moreover, the developed formulation in literature is generally limited to a given combination of dipole orientation, position, and region of interest.

Then, as far as we know, there is not a single publication that conveys the magnetic field expressions valid from the near to the far region. In addition, despite that evaluating Sommerfeld integrals can be a routine task with the use of the contemporary computers in conjunction with the advent of algorithms to speed the calculations (Chew et al., 2001; Hochman & Leviatan, 2010), a specific integration strategy directly applicable to subsurface applications is not available.

Consequently, in this paper, the explicit magnetic field expressions for a magnetic dipole source (VMD and HMD) for any source-observer configuration for a three-layered medium model valid from the near zone to the far zone are presented. The magnetic field components due to an arbitrary oriented dipole source can be derived in a well-known manner. Then, an integration routine is presented to accurately evaluate the integral solutions. We validate the expressions to compute and routine employed by comparisons using FEM simulations. Finally, two cases of study are presented to show the usefulness of the developed channel model. An implementation of the field expressions and integration routine is freely available for download (Ayuso & Lera, 2019).

2. Magnetic Field of a Magnetic Dipole in a Three-Layered Region

In Figure 1, the general description of the problem considered in this paper is illustrated. The air occupies the region $z \geq 0$ where we assume ideal vacuum properties. The interface at $z = 0$ is the upper edge of a homogeneous medium, Region 1, of conductivity σ_1 and relative permittivity ϵ_{r1}. The lower interface is at $z = -d$, corresponding to the surface of a homogeneous medium, Region 2, of conductivity σ_2 and relative permittivity ϵ_{r2}. It is supposed that both Region 1 and Region 2 are nonmagnetic so that $\mu_1 = \mu_2 = \mu_0 = 4\pi \times 10^{-7}$ H/m.

The magnetic dipole source can be placed anywhere on the z axis $(0, 0, z')$ with an arbitrary orientation, α, with respect to the vertical axis. This can be decomposed into a VMD and an HMD dipole as shown in Figure 1. Solutions for the VMD source, when the dipole is oriented in the z direction, are derived in cylindrical coordinates (ρ, ϕ, z), with base vectors $(\hat{\boldsymbol{\rho}}, \hat{\boldsymbol{\phi}}, \hat{\mathbf{z}})$, due to the axial symmetry of the problem. The HMD is oriented in the y direction and the Cartesian coordinate system (x, y, z), with base vectors $(\hat{\mathbf{x}}, \hat{\mathbf{y}}, \hat{\mathbf{z}})$, is used.

Finally, the dipole sources vary time-harmonic according to $e^{+j\omega t}$, where ω is the angular frequency and t is time. This term is implied throughout this work. The International System of units is employed.

2.1. Derivation of Fields

The procedure used to derive the magnetic field expressions for the VMD and HMD sources follows the work by Burke and Jones for the electrical dipole and the source placed in the central layer (Burke & Jones, 1994).

First, we define the Hertz vector $\prod^*$ that solves the wave equation according to the dipole source (VMD or HMD), that is, the Green's functions. In the region where the source is placed, the Hertz vector is suitably split as primary and secondary potential terms written as Sommerfeld integrals using the Fourier-Bessel transforms (Sommerfeld, 1926),

$$\frac{e^{-jkR}}{R} = \int_0^\infty \frac{\lambda}{u} e^{-u|z-z'|} J_0(\lambda\rho)\mathrm{d}\lambda \tag{1}$$

where $R = \sqrt{\rho^2 + (z-z')^2}$ is the distance between the source and the observation point, $k = \omega\sqrt{\mu_0\left(\epsilon_0\epsilon_r - j\sigma/\omega\right)}$ is the wave number, and $u = \sqrt{\lambda^2 - k^2}$ is taken with positive real part in order to ensure the convergence of the integral and its vanishing for z to plus or minus infinity. Further, λ is the integration parameter and must not be confused with the wavelength.

At this point, it is relevant to notice that the evaluation of the Sommerfeld integrals appearing in field expressions is numerically intended. Numerical integration can be helped by integrands that are less oscillatory. To do this, factors normalized to a parameter pertained to the geometry of the problem can be helpful. In the present work, the field expressions are first transformed by normalization with a convenient scaling length, h. Consequently, the integration variable λ is changed to $\lambda' = \lambda \cdot h$. In the past, the choice of h was somewhat arbitrary. In section 4, the adequate choice of the normalization parameter in the general source observation case will be considered.

Now, following the method of solution, for the VMD case, only a z component of the Hertz vector is needed. For the HMD (y oriented), an additional z component must be introduced apart from the y component in order to satisfy the boundary conditions.

Second, we apply the boundary conditions, that is, continuity of the tangential components of the electric and magnetic fields to obtain the unknown coefficients.

Finally, we derive the magnetic field expressions from the magnetic Hertz vector potential (Stratton, 1941).

In the region where the source is placed, the total value of any field component is computed by adding together the primary and secondary components. Otherwise, the field is only due to the secondary components. The former are given in (2)–(4) and (22)–(24) for the VMD and the HMD, respectively. They are the values of the field in a medium of infinite extent. The corresponding secondary explicit field expressions for any source-observer configuration are given in (5)–(7) and (25)–(27). The region where the source is located determines the coefficients in (8)–(19) and (28)–(51).

Note that formulation for the half-space model is straightforwardly derived from these expressions by matching the electrical properties of Regions 1 and 2.

In the interest of representing the secondary contributions in a compact form, the following convention has been adopted: the region where the source is placed is indicated by the subscript i: $i = 0$ accounts for the air, $i = 1$ for the intermediate layer, and $i = 2$ for the deepest layer.

2.2. VMD Formulation

The primary field expressions from a VMD source, z axis oriented, immersed in an unbounded medium are well known (Stratton, 1941; Wait, 1969):

$$H_\rho = -\frac{IdA}{4\pi}\rho\left(z-z'\right)\left(\frac{k_i^2}{R^2} - \frac{3jk_i}{R^3} - \frac{3}{R^4}\right)\frac{e^{-jk_iR}}{R} \tag{2}$$

$$H_\phi = 0 \tag{3}$$

$$H_z = \frac{IdA}{4\pi}\left[k_i^2 - \frac{jk_i}{R} - \frac{1}{R^2} - (z-z')^2\left(\frac{k_i^2}{R^2} - \frac{3jk_i}{R^3} - \frac{3}{R^4}\right)\right]\frac{e^{-jk_iR}}{R} \tag{4}$$

where IdA is the magnetic moment due to a small loop of current of area dA and circulating current I. The secondary fields from a VMD are given in (5)–(7),

$$H_\rho^s = \begin{cases} \frac{IdA}{4\pi h^3}\int_0^\infty \lambda' h u_0 L_i e^{-u_0 z} J_1\left(\frac{\lambda'}{h}\rho\right) d\lambda' & z \geq 0 \\ \frac{IdA}{4\pi h^3}\int_0^\infty \lambda' h u_1 \left(-M_i e^{u_1 z} + N_i e^{-u_1 z}\right) J_1\left(\frac{\lambda'}{h}\rho\right) d\lambda' & 0 < z \leq -d \\ -\frac{IdA}{4\pi h^3}\int_0^\infty \lambda' h u_2 P_i e^{u_2 z} J_1\left(\frac{\lambda'}{h}\rho\right) d\lambda' & z < -d \end{cases} \tag{5}$$

$$H_\phi^s = 0 \qquad -\infty < z < \infty \tag{6}$$

$$H_z^s = \begin{cases} \frac{IdA}{4\pi h^3}\int_0^\infty \lambda'^2 L_i e^{-u_0 z} J_0\left(\frac{\lambda'}{h}\rho\right) d\lambda' & z \geq 0 \\ \frac{IdA}{4\pi h^3}\int_0^\infty \lambda'^2 \left(M_i e^{u_1 z} + N_i e^{u_1 z}\right) J_0\left(\frac{\lambda'}{h}\rho\right) d\lambda' & 0 < z \leq -d \\ \frac{IdA}{4\pi h^3}\int_0^\infty \lambda'^2 P_i e^{u_2 z} J_0\left(\frac{\lambda'}{h}\rho\right) d\lambda' & z < -d \end{cases} \tag{7}$$

where the coefficients determined from the boundary conditions are

$$L_0 = -\frac{\lambda'}{h}\frac{1}{u_0}e^{-u_0|z'|} + M_0 + N_0 \tag{8}$$

$$M_0 = R_{10}C_0 + T_{01}\frac{\lambda'}{h}\frac{1}{u_0}e^{-u_0|z'|} \tag{9}$$

$$N_0 = T_{01}R_{12}\left(\frac{\frac{\lambda'}{h}\frac{1}{u_0}e^{-2u_1 d}e^{-u_0|z'|}}{1 - R_{10}R_{12}e^{-2u_1 d}}\right) \tag{10}$$

$$P_0 = e^{u_2 d}\left(M_0 e^{-u_1 d} + N_0 e^{u_1 d}\right) \tag{11}$$

$$L_1 = \frac{\lambda'}{h}\frac{1}{u_1}e^{-u_1|z'|} + M_1 + N_1 \tag{12}$$

$$M_1 = \frac{\lambda'}{h}\frac{1}{u_1}e^{-u_1|z'|}R_{10}\left(\frac{1 + R_{12}e^{-2u_1(d-|z'|)}}{1 - R_{10}R_{12}e^{-2u_1 d}}\right) \tag{13}$$

$$N_1 = \frac{\lambda'}{h}\frac{1}{u_1}e^{-u_1(2d-|z'|)}R_{12}\left(\frac{1 + R_{10}e^{-2u_1|z'|}}{1 - R_{10}R_{12}e^{-2u_1 d}}\right) \tag{14}$$

$$P_1 = e^{u_2 d}\left(\frac{\lambda'}{h}\frac{1}{u_1}e^{-u_1(d-|z'|)} + M_1 e^{-u_1 d} + N_1 e^{u_1 d}\right) \tag{15}$$

$$L_2 = M_2 + N_2 \tag{16}$$

$$M_2 = R_{10}N_2 \tag{17}$$

$$N_2 = T_{21}\left(\frac{\frac{\lambda'}{h}\frac{1}{u_2}e^{u_2(d-|z'|)}e^{-u_1 d}}{1 - R_{10}R_{12}e^{-2u_1 d}}\right) \tag{18}$$

$$P_2 = e^{u_2 d}\left(-\frac{\lambda'}{h}\frac{1}{u_2}e^{u_2(d-|z'|)} + M_2 e^{-u_1 d} + N_2 e^{u_1 d}\right) \tag{19}$$

The corresponding transmission and reflection coefficients are functionally the same as those defined for transverse electric waves or horizontally polarized waves incident onto layer j from layer i,

$$R_{ij} = \frac{u_i - u_j}{u_i + u_j} \tag{20}$$

$$T_{ij} = \frac{2u_i}{u_i + u_j} \tag{21}$$

2.3. HMD Formulation

The primary field expressions from a HMD source, y axis, immersed in an unbounded medium, in Cartesian coordinate system are

$$H_x = \frac{IdA}{4\pi}\left(\frac{3}{R^3} + \frac{3jk_i}{R^2} - \frac{k_i^2}{R}\right)\frac{xy}{R^2}e^{-jk_i R} \tag{22}$$

$$H_y = \frac{IdA}{4\pi}\left[\left(\frac{3}{R^3} + \frac{3jk_i}{R^2} - \frac{k_i^2}{R}\right)\frac{y^2}{R^2} - \left(\frac{1}{R^3} + \frac{jk_i}{R^2} - \frac{k^2}{R}\right)\right]e^{-jk_i R} \tag{23}$$

$$H_z = \frac{IdA}{4\pi}\left(\frac{3}{R^3} + \frac{3jk_i}{R^2} - \frac{k^2}{R}\right)\frac{y(z-z')}{R^2}e^{-jk_i R} \tag{24}$$

The secondary field expressions are given in (25)–(27)

$$H_x^s = \begin{cases} \frac{IdA}{4\pi h^3}\int_0^\infty \left(-A_i + u_0 R_i\right)e^{-u_0 z}\frac{\lambda' hxy}{\rho^2}\left[\frac{\lambda'}{h}J_0(\frac{\lambda'}{h}\rho) - \frac{2}{\rho}J_1\left(\frac{\lambda'}{h}\rho\right)\right]d\lambda' & z \geq 0 \\ -\frac{IdA}{4\pi h^3}\int_0^\infty \left[\left(B_i e^{u_1 z} + C_i e^{-u_1 z}\right) + u_1\left(S_i e^{u_1 z} - T_i e^{-u_1 z}\right)\right]\times \\ \frac{\lambda' hxy}{\rho^2}\left[\frac{\lambda'}{h}J_0\left(\frac{\lambda'}{h}\rho\right) - \frac{2}{\rho}J_1\left(\frac{\lambda'}{h}\rho\right)\right]d\lambda' & 0 < z \leq -d \\ -\frac{IdA}{4\pi h^3}\int_0^\infty \left(D_i + u_2 V_i\right)e^{u_2 z}\frac{\lambda' hxy}{\rho^2}\left[\frac{\lambda'}{h}J_0\left(\frac{\lambda'}{h}\rho\right) - \frac{2}{\rho}J_1\left(\frac{\lambda'}{h}\rho\right)\right]d\lambda' & z < -d \end{cases} \tag{25}$$

$$H_y^s = \begin{cases} \frac{IdA}{4\pi h^3}\int_0^\infty \left\{h^2 k_0^2 A_i e^{-u_0 z}J_0\left(\frac{\lambda'}{h}\rho\right) + \right. \\ \left.\left(-A_i + u_0 R_i\right)e^{-u_0 z}\left[\frac{\lambda'^2 y^2}{\rho^2}J_0\left(\frac{\lambda'}{h}\rho\right) + \lambda' h\left(\frac{1}{\rho} - \frac{2y^2}{\rho^3}\right)J_1\left(\frac{\lambda'}{h}\rho\right)\right]\right\}d\lambda' & z \geq 0 \\ \frac{IdA}{4\pi h^3}\int_0^\infty \left\{k_1^2 h^2\left(B_i e^{u_1 z} + C_i e^{-u_1 z}\right)J_0\left(\frac{\lambda'}{h}\rho\right) + \right. \\ \left[-\left(B_i e^{u_1 z} + C_i e^{-u_1 z}\right) + u_1(S_i e^{u_1 z} - T_i e^{-u_1 z})\right]\times \\ \left.\left[\frac{\lambda'^2 y^2}{\rho^2}J_0\left(\frac{\lambda'}{h}\rho\right) + \lambda' h\left(\frac{1}{\rho} - \frac{2y^2}{\rho^3}\right)J_1\left(\frac{\lambda'}{h}\rho\right)\right]\right\}d\lambda' & 0 < z \leq -d \\ \frac{IdA}{4\pi h^3}\int_0^\infty \left\{h^2 k_2^2 D_i e^{u_2 z}J_0\left(\frac{\lambda'}{h}\rho\right) + \right. \\ \left.\left(-D_i - u_2 V_i\right)e^{u_2 z}\left[\frac{\lambda'^2 y^2}{\rho^2}J_0\left(\frac{\lambda'}{h}\rho\right) + \lambda' h\left(\frac{1}{\rho} - \frac{2y^2}{\rho^3}\right)J_1\left(\frac{\lambda'}{h}\rho\right)\right]\right\}d\lambda' & z < -d \end{cases} \tag{26}$$

$$H_z^s = \begin{cases} \frac{IdA}{4\pi h^3}\int_0^\infty \left(u_0 A_i - \frac{\lambda'^2}{h^2}R_i\right)e^{-u_0 z}\frac{\lambda' hy}{\rho}J_1\left(\frac{\lambda'}{h}\rho\right)d\lambda' & z \geq 0 \\ -\frac{IdA}{4\pi h^3}\int_0^\infty \left[u_1\left(B_i e^{u_1 z} - C_i e^{-u_1 z}\right) + \frac{\lambda'^2}{h^2}\left(S_i e^{u_1 z} + T_i e^{-u_1 z}\right)\right]\times \\ \frac{\lambda' hy}{\rho}J_1\left(\frac{\lambda'}{h}\rho\right)d\lambda' & 0 < z \leq -d \\ -\frac{IdA}{4\pi h^3}\int_0^\infty \left(u_2 D_i + \frac{\lambda'^2}{h^2}V_i\right)e^{u_2 z}\frac{\lambda' hy}{\rho}J_1\left(\frac{\lambda'}{h}\rho\right)d\lambda' & z < -d \end{cases} \tag{27}$$

From the boundary conditions at the interfaces, the unknown coefficients are

$$A_0 = \frac{k_1^2}{k_0^2} T_{10}^{||} C_0 + R_{01}^{||} \frac{\lambda'}{h} \frac{1}{u_0} e^{-u_0|z'|} \tag{28}$$

$$B_0 = R_{10}^{||} C_0 + \left(\frac{2k_0^2 u_0}{k_0^2 u_1 + k_1^2 u_0} \right) \frac{\lambda'}{h} \frac{1}{u_0} e^{-u_0|z'|} \tag{29}$$

$$C_0 = \frac{\lambda\prime}{h} \frac{1}{u_0} e^{-u_0|z\prime|} e^{-2u_1 d} R_{12}^{||} \left(\frac{\frac{2k_0^2 u_0}{k_1^2 u_0 + k_0^2 u_1}}{1 - R_{10}^{||} R_{12}^{||} e^{-2u_1 d}} \right) \tag{30}$$

$$D_0 = e^{u_2 d} \frac{k_1^2}{k_2^2} \left(B_0 e^{-u_1 d} + C_0 e^{u_1 d} \right) \tag{31}$$

$$R_0 = S_0 + T_0 \tag{32}$$

$$S_0 = R_{10} T_0 + \frac{k_1^2 - k_0^2}{k_0^2 u_1 + k_1^2 u_0} \left(T_{10} C_0 + T_{01} \frac{\lambda'}{h} \frac{1}{u_0} e^{-u_0|z'|} \right) \tag{33}$$

$$\begin{aligned} T_0 = {} & \frac{1}{u_1 + u_2} \\ & \times \left(\frac{\frac{\lambda\prime}{h} \frac{1}{u_0} e^{-u_0|z\prime|} e^{-2u_1 d}}{1 - R_{10} R_{12} e^{-2u_1 d}} \right. \\ & \times \left[T_{01} R_{12} \left(u_1 + u_2 \right) \frac{k_1^2 - k_0^2}{k_0^2 u_1 + k_1^2 u_0} + \frac{2k_0^2 u_0}{k_0^2 u_1 + k_1^2 u_0} \right] \\ & + \frac{C_0}{1 - R_{10} R_{12} e^{-2u_1 d}} \\ & \times \left\{ \left[R_{10}^{||} + T_{10} R_{12} \left(u_1 + u_2 \right) \frac{k_1^2 - k_0^2}{k_0^2 u_1 + k_1^2 u_0} \right] e^{-2u_1 d} + 1 \right\} \\ & \left. - \frac{D_0 e^{-d(u_1 + u_2)}}{1 - R_{10} R_{12} e^{-2u_1 d}} \right) \end{aligned} \tag{34}$$

$$V_0 = e^{u_2 d} \left(S_0 e^{-u_1 d} + T_0 e^{u_1 d} \right) \tag{35}$$

$$A_1 = \frac{k_1^2}{k_0^2} T_{10}^{||} \left(C_1 + \frac{\lambda'}{h} \frac{1}{u_1} e^{-u_1|z'|} \right) \tag{36}$$

$$B_1 = R_{10}^{||} \left(C_1 + \frac{\lambda'}{h} \frac{1}{u_1} e^{-u_1|z'|} \right) \tag{37}$$

$$C_1 = R_{12}^{||} \frac{\frac{\lambda'}{h} \frac{1}{u_1} e^{-u_1|d-|z'||} e^{-u_1 d} + R_{10}^{||} \frac{\lambda'}{h} \frac{1}{u_1} e^{-u_1(2d+|z'|)}}{1 - R_{10}^{||} R_{12}^{||} e^{-2u_1 d}} \tag{38}$$

$$D_1 = \frac{k_1^2}{k_2^2} e^{u_2 d} \left(\frac{\lambda'}{h} \frac{1}{u_1} e^{-u_1|d-|z'||} + B_1 e^{-u_1 d} + C_1 e^{u_1 d} \right) \tag{39}$$

$$R_1 = S_1 + T_1 \tag{40}$$

$$S_1 = R_{10} T_1 + T_{10} \frac{k_1^2 - k_0^2}{k_0^2 u_1 + k_1^2 u_0} \left(C_1 + \frac{\lambda'}{h} \frac{1}{u_1} e^{-u_1|z'|} \right) \tag{41}$$

$$T_1 = \frac{1}{u_1+u_2} \times \left\{ \frac{\frac{\lambda\prime}{h}\frac{1}{u_1}e^{-u_1(2d+|z\prime|)}}{1-R_{10}R_{12}e^{-2u_1d}} \times \left[R_{10}^{||} + T_{10}R_{12}\left(u_1+u_2\right)\frac{k_1^2-k_0^2}{k_0^2u_1+k_1^2u_0} \right] + \frac{\frac{\lambda\prime}{h}\frac{1}{u_1}e^{-u_1|d-|z\prime||}e^{-u_1d}}{1-R_{10}R_{12}e^{-2u_1d}} + \frac{\left\{ \left[R_{10}^{||} + T_{10}R_{12}\left(u_1+u_2\right)\frac{k_1^2-k_0^2}{k_0^2u_1+k_1^2u_0} \right] e^{-2u_1d}+1 \right\} C_1}{1-R_{10}R_{12}e^{-2u_1d}} - \frac{D_1e^{-d(u_1+u_2)}}{1-R_{10}R_{12}e^{-2u_1d}} \right\} \tag{42}$$

$$V_1 = e^{u_2d}\left(S_1e^{-u_1d} + T_1e^{u_1d}\right) \tag{43}$$

$$A_2 = \frac{k_1^2}{k_0^2}T_{10}^{||}C_2 \tag{44}$$

$$B_2 = R_{10}^{||}C_2 \tag{45}$$

$$C_2 = \frac{\lambda\prime}{h}\frac{1}{u_2}e^{u_2(d-|z\prime|)}e^{-u_1d}\frac{\frac{2k_2^2u_2}{k_1^2u_2+k_2^2u_1}}{1-R_{10}^{||}R_{12}^{||}e^{-2u_1d}} \tag{46}$$

$$D_2 = e^{u_2d}\left[\frac{k_1^2}{k_2^2}\left(B_2e^{-u_1d}+C_2e^{u_1d}\right) - \frac{\lambda\prime}{h}\frac{1}{u_2}e^{u_2(d-|z\prime|)}\right] \tag{47}$$

$$R_2 = S_2 + T_2 \tag{48}$$

$$S_2 = R_{10}T_2 + T_{10}\frac{k_1^2-k_0^2}{k_0^2u_1+k_1^2u_0}C_2 \tag{49}$$

$$T_2 = \frac{1}{u_1+u_2}\left(-\frac{\frac{\lambda\prime}{h}\frac{1}{u_2}e^{u_2(d-|z\prime|)}e^{-u_1d}}{1-R_{10}R_{12}e^{-2u_1d}} + \frac{\left\{ \left[R_{10}^{||} + T_{10}R_{12}\left(u_1+u_2\right)\frac{k_1^2-k_0^2}{k_0^2u_1+k_1^2u_0} \right] e^{-2u_1d}+1 \right\} C_2}{1-R_{10}R_{12}e^{-2u_1d}} - \frac{D_2e^{-d(u_1+u_2)}}{1-R_{10}R_{12}e^{-2u_1d}} \right) \tag{50}$$

$$V_2 = e^{u_2d}\left(S_2e^{-u_1d} + T_2e^{u_1d}\right) \tag{51}$$

where the transmission and reflection coefficients are functionally the same as those defined for transverse magnetic waves or vertically polarized waves incident onto layer j from layer i,

$$R_{ij}^{||} = \frac{k_j^2u_i - k_i^2u_j}{k_j^2u_i + k_i^2u_j} \tag{52}$$

$$T_{ij}^{||} = \frac{2k_j^2u_i}{k_j^2u_i + k_i^2u_j} \tag{53}$$

Table 1
Electrical Properties for Subsurface Applications

Symbol	Quantity	Unit	Air	Region 1,2
σ_i	Conductivity	S/m	0	$[0.2 \cdot 10^{-3}$ to $10^{0}]$
μ_i	Permeability	H/m	$4\pi \times 10^{-7}$	$4\pi \times 10^{-7}$
ϵ_0	Permittivity	F/m	8.854×10^{-12}	8.854×10^{-12}
ϵ_r	Relative permittivity		1	[4–50]

2.4. Arbitrarily Oriented Magnetic Dipole Formulation

The field solutions for an arbitrary oriented dipole with respect to the z axis can be obtained by decomposing the source dipole moment into vertical and horizontal components, see Figure 1. Therefore, any field component is given by the simple vector representation,

$$H_i = H_i^{\mathrm{VMD}} \cdot \cos(\alpha) + H_i^{\mathrm{HMD}} \cdot \sin(\alpha) \tag{54}$$

where α is the angle to the vertical (z direction), i refers to the x, y, or z field component if the Cartesian coordinate system is selected. H_i^{VMD} and H_i^{HMD} are the magnetic field solutions for the VMD and HMD sources depicted in (5)–(7) and (25)–(27), respectively. Notice that in this case the VMD solutions have to be transformed into Cartesian coordinate system.

3. Proposed Integration Algorithm

The resultant field solutions expressed in terms of Sommerfeld-type integrals are difficult to evaluate due to their oscillating infinite nature. Since these integrals were introduced, many studies have been conducted in order to develop accurate and efficient quadrature numerical methods for their evaluation (Fraser-Smith & Bubenik, 1976). Nowadays, there are efficient computation algorithms that yield high accuracy results for oscillatory integrands over infinite integration intervals (Gander & Gautschi, 2000; Shampine, 2008).

For this work, we used the adaptive quadrature method implemented in *integral* function in MATLAB (MATLAB). The field equations presented in section 2 were rewritten with the aid of symbolic mathematical manipulation software to simplify the expressions and to avoid divergent exponentials. The former reduces computation time and the latter prevents infinite factors in the integrands.

The objective is to guarantee that the numerical integration gives accurate results for subsurface applications with the electrical parameters and geometry shown in Tables 1 and 2, respectively.

To this end, an integration routine was defined. The routine has taken into account the following aspects: the integration limit, the absolute and relative tolerances, and the use of a normalization parameter h.

First, in order to establish the integration upper limit, it is possible to analyze the integrand to determine a proper bound. We compare the computational time and accuracy when using a specific precalculated limit or setting it to "Inf." As a result, the "Inf" required lower computational times and accurate results. Consequently, this is used by default for the numerical integration.

Second, the absolute and relative tolerances settings were studied. We found that the relative error tolerance was limited to $2.22 \cdot 10^{-14}$ and the absolute error tolerance allowed higher accuracies. Consequently, the relative error tolerance was set to 0 for pure absolute error tolerance use. After evaluating different limiting cases, we set this value a the minimum between 10^{-16} (the default value is 10^{-10} in double precision) and the tenth value of the previous calculated field component. This gave accurate results when the field was computed from near to far distances from the source.

Table 2
Geometric Variables

Symbol	Quantity	Unit	Range
z'	source z coordinate	m	[−100–10]
z	observer z coordinate	m	[−100–10]
ρ	source-observer radial distance	m	<1,000

Moreover, as stated in the previous section, present formulation includes a transformation of the integration constant by the parameter h. In the literature, different values of h have been used depending on the geometry of the problem, that is, $h = |z'|$ by Wait (1972), Durkin (1983), and Shope (1983); $h = |z|$ by Wait and Spies (1971, 1972) and Durkin (1983); $h = \delta$ by Wait (1982), where δ is the skin depth, or $h = 1/|k|$ by Abo-Seida (2002), where k is the wave number. In order to determine the optimal selection of h, its effects on computation time and accuracy for any source-observer configuration were analyzed. With the use of the *integral* function in MATLAB we realized that no relevant differences were observed. However, as the integrand is less oscillatory when $h > 1$, optionally, this parameter can be used according to the following rules. For a source placed in air, h must be set to the depth of the observation point, $|z|$. In case of a buried emitter, h must be set to the source depth $|z'|$. For a resultant $h < 1$ and the remaining source-observer combinations, the numerical integration performed better by setting h to 1. These outcomes are analyzed in detail in Ayuso (2010).

Notice that this routine is focused on the accuracy of the results for a general subsurface application and does not try to speed-up calculations. To this end, many works on the topic can be found in the literature (Hochman & Leviatan, 2010; Long et al., 2001; Wei et al., 2011).

Finally, the code for the field expressions and integration algorithm is freely available from Ayuso and Lera (2019).

4. Results and Comparison

In the former literature, the validation tests for the derived field solutions were limited to a reduced number of calculations. The methods used for validation included comparisons with the asymptotic evaluation of the Sommerfeld integrals as in Raj Mittra and Rahmat-Samii (1979) or the exact Sommerfeld integration when possible (Bannister, 1981; Raj Mittra & Rahmat-Samii, 1979). For applications in the lowest band of the spectrum, they involved comparison with the static results (Burke & Jones, 1994). Besides, as the tangential components of the field should be continuous across the interfaces, this check was also used.

Nowadays, the FEM can be applied to model through-the-Earth propagation. Therefore, a comprehensive analysis of validity can be conducted. In the present work, the numerical integration of the field expressions was tested by FEM computations using the COMSOL Multiphysics package COMSOL. The goodness of fit between both numerical data was based on the normalized root-mean-square error (NRMSE). The fitness metric is defined as

$$fit(z) = 1 - \frac{\|Hi_{\text{Num\_Int}}(:,z) - Hi_{\text{FEM}}(:,z)\|}{\|Hi_{\text{Num\_Int}}(:,z) - \text{mean}(Hi_{\text{Num\_Int}}(:,z))\|} \tag{55}$$

where $H_i(:,z)$ is the magnetic field intensity i component at elevation z along the distances between the source and observation points taken into account, $\|\cdot\|$ indicates the two norm of a vector, and fit is a scalar value. The numerical integration results ($Hi_{\text{Num\_Int}}(:,z)$) are considered the model reference and the FEM computations ($Hi_{\text{FEM}}(:,z)$), the test data. The NRMSE can vary between $-\infty$ (bad fit) to 1 (perfect fit).

The study includes three frequencies in the range of representative underground applications: 1 kHz, 100 KHz, and 10 MHz. That is, the lowest frequency is specially intended for subsurface location whereas the highest ones are close to the candidates in the low-frequency industrial, scientific, and medical bands for underground communications due to its lower attenuation. Typical soil characteristics have been chosen: Region 1 of width 5 m and electrical parameters $\sigma = 10$ mS/m and $\epsilon_r = 8$ and Region 2 with $\sigma = 1$ mS/m and $\epsilon_r = 4$. Therefore, as the test is conducted to a distance from the source to about 100 m, depending on the operating frequency and region of interest, the study covers from the near- to well within the far-field region. For example, in order to satisfy $|kR| \ll 1$, it follows that in Region 1, the near-zone limit is 500, 50, and 5 m at 1 KHz, 100 KHz, and 10 MHz, respectively.

4.1. VMD Results

The Sommerfeld integrals have been evaluated at any source-observation combination. The emitter has been placed at positions in the three layers, $z' = 1$ m for the air, $z' = -2$ m for Region 1, and $z' = -7$ m for Region 2. Then, for any field component, the observation points have been placed at $z = 1, -2$, and -7 m and radial coordinates from 0 to 100 m with a step size of 1 m. All the simulations were performed in an Intel Core i7-2600 CPU at 3.40 GHz with 16 Gb of RAM. A total execution time of approximately 1,000 s was required for the numerical evaluation of 600 integrals.

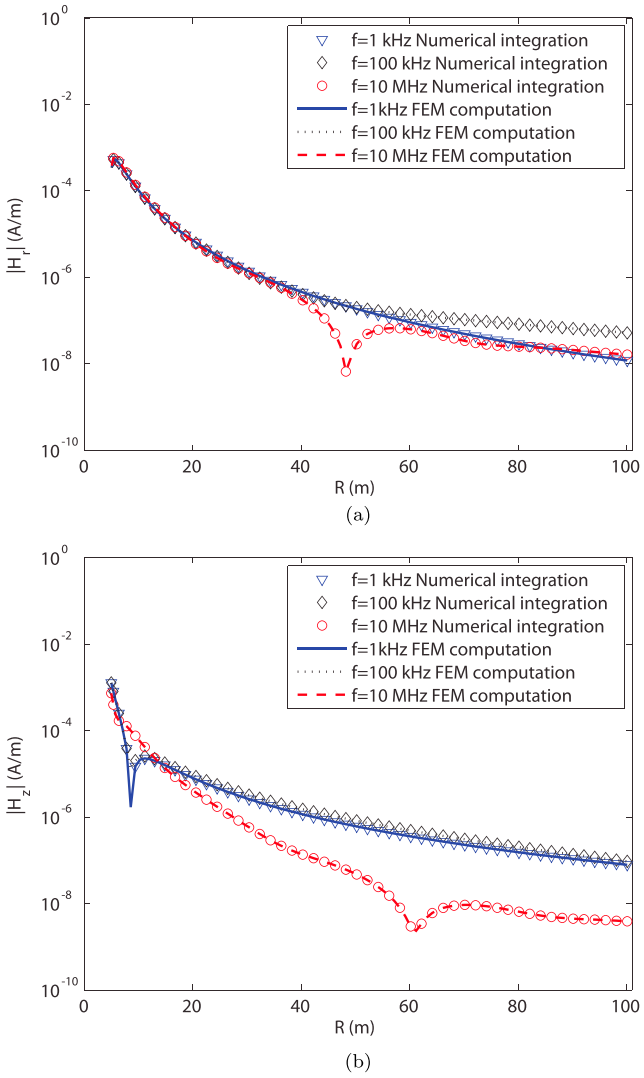

Figure 2. Radial (a) and axial (b) components of the magnetic fields of a vertical magnetic dipole as a function of the distance in the presence of a soil layer with $d = 5$ m. The dipole is located on z axis in the lower soil region at $z' = -7$ m and the observation points at the upper soil region $z = -2$ m. FEM = Finite Element Method.

The corresponding FEM models can be two-dimensional due to the axial symmetry of the problem in the VMD case. This allows a very dense mesh with low computational requirements and solver time. Therefore, very accurate solutions can be obtained because the accuracy of the solution is linked to the mesh size. Primarily, at any frequency, the mesh size and truncation of the model geometry had to be analyzed in order to set the valid FEM reference model. Figure 2 presents FEM and MATLAB results graphically. Table 3 shows the 100-kHz mesh study results. Column DOF (degrees of freedom) is related to the problem size due

Table 3
Mesh Study at 100 kHz

Elements/Wavelength	DOF	Solution time	Fit H_ρ	Fit H_z
5	78910	8 s	−14.058	−901.078
8	106861	10 s	0.992	0.816
8 + refinement	123808	11 s	0.999	0.998

Note. Emitter at Region 2 ($z' = -7$ m) and receiver at Region 1 ($z = -2$ m); DOF = degrees of freedom.

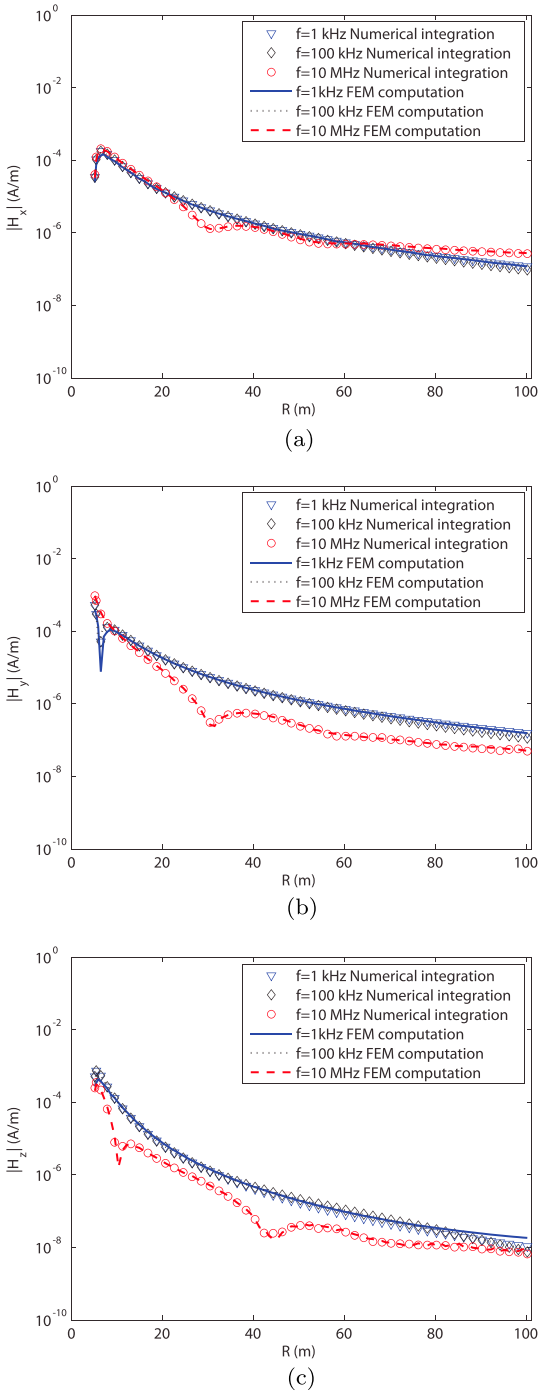

Figure 3. (a) H_x, (b)H_y, and (c) H_z components of the magnetic fields of a horizontal magnetic dipole as a function of the distance in the presence of a soil layer with $d = 5$ m. The dipole is located on z axis in the lower soil region at $z' = -7$ m and the observation points at the upper soil region $z = -2$ m. H_x is studied at $\phi = \pi/4$, H_y, and H_z along the y axis. FEM = Finite Element Method.

to the meshing type as the shape functions (approximation of the unknown solution within an element) and the number of dependent variables in the model are constant. As can be observed, a mesh size of eight elements per wavelength and a refinement in the area where the solution was intended was enough for accurate results. In order to reduce the problem size, the truncation of the geometry was also studied. We used a perfectly matched layer to absorb the incident radiation without producing reflection for an accurate

Table 4
Computing Requirements for the HMD

Frequency	DOF	RAM	Solution time
1 kHz	1,236,542	7.5 GB	1 hr 30 min
100 kHz	1,177,842	4 GB	15 min
10 MHz	6,654,400	34 GB	2 hr 30 min

solution. As a result, the desired accuracy was achieved, $fit \approx 1$, with low computational requirements and solution time.

4.2. HMD Results

The same problem is analyzed for a HMD of unity magnetic moment oriented in the y direction. Figure 3 shows the field components at directions where the field intensity is relevant. Therefore, H_x has been analyzed at $\phi = \pi/4$ and H_y and H_z along the y axis.

Numerical integration times were similar to those of the VMD case. However, FEM models in this case are highly demanding three-dimensional problems despite of its symmetry. Although the geometry was halved, it was very big for the 1-kHz frequency due to the required truncation limits and the 10-MHz frequency due to its size in comparison to the wavelength. In both cases, computing requirements exceeded our desktop computer capabilities and the calculus had to be carried out into a high-performance node of the computer cluster HERMES hosted by the Aragón Institute of Engineering Research (I3A). Presently, HERMES consists of 200 computing nodes with a total amount of 1,534 cores and 3.5 Tb of RAM. Among them, a node with a Quad 12-core AMD Magny-Cours 6174 at 2.1 Ghz and 96 Gb of RAM was used for the FEM simulations. Table 4 shows, for any frequency, the DOF of the problem and the required memory and computing time in the cluster in mean for the three emitter positions. As a result, a good fit in mean, $fit \approx 0.9$, was achieved for 100 kHz and 10 MHz. However, at 1 kHz, truncation effects were evident as can be observed at the H_z component of Figure 3 giving a mean $fit \approx 0.7$. The biggest problem we could manage for 1 kHz was 3.6 millions of DOF and was solved in 5 hr using 22 GB of RAM. Although truncation effects were reduced, the solution in the proximity of the source was worse because of the resultant poorer mesh quality.

5. Study Cases

Following, two challenging applications of wireless underground sensor networks (WUSNs) are considered. The objective is to show the usefulness of the proposed field computation algorithms.

5.1. Underground Communications

WUSNs are a growing area of interest due to it wide variety of novel applications (Akyildiz & Stuntebeck, 2006b; Tan et al., 2015; Vuran et al., 2018). Among different technologies, MI has been considered to allow communications between small coils in buried environments (Sun & Akyildiz, 2010).

To date, MI channel has been usually modeled using MI-Tx and Rx circuits as a whole (Lin et al., 2015; Sun & Akyildiz, 2010; 2012). A novel approach separates the Tx and Rx circuits to better characterize the signal attenuation but considers the media unbounded (Silva & Moghaddam, 2015).

In the following, we are showing the channel attenuation for a MI-based subsurface application consisting on soil condition monitoring as in "smart agriculture." The aim of the simulations is to take into account the boundary effects as in the case of EM waves (Dong & Vuran, 2011; Vuran & Akyildiz, 2010).

In Figure 4 the received magnetic field for two horizonal dipoles buried at three shallow depths from the interface is calculated according the free

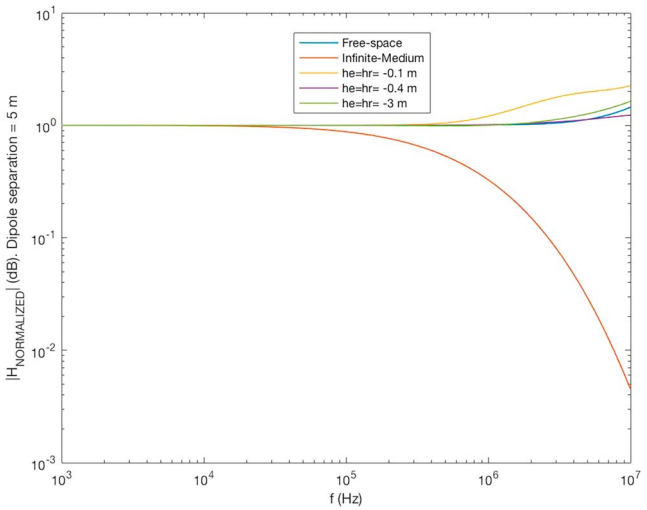

Figure 4. Normalized received field for basic propagation models. HMD buried at different shallow depths.

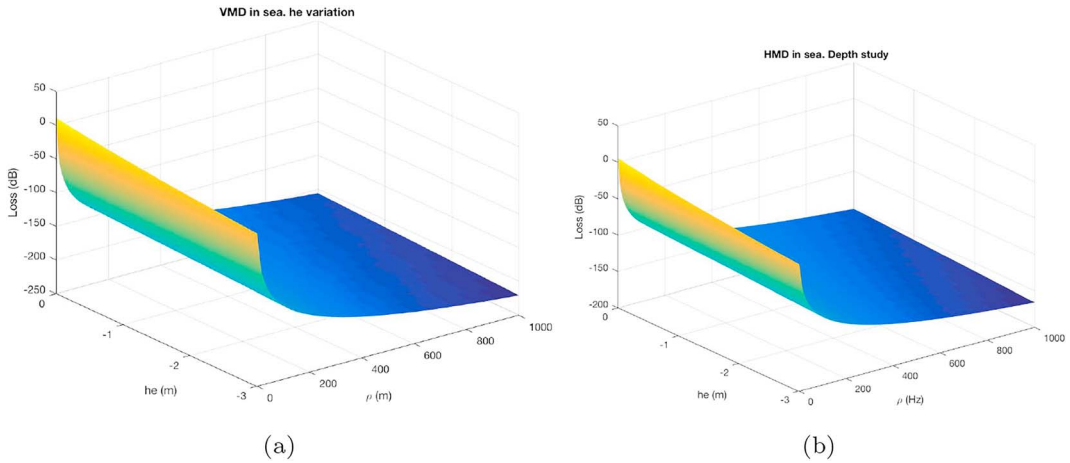

Figure 5. Magnetic dipole buried in seawater. Receiver at $z = 1.5$ m. Absolute magnetic field versus the burial depth and horizontal distance. (a) vertical magnetic dipole (VMD); (b) horizontal magnetic dipole (HMD).

space, infinite medium, and three-layered model. For the simulations, conductivity of medium 1 is set to 70 mS/m and relative permittivity of 12. Medium 2 is set to 0.5 mS/m and relative permittivity of 2 (Vuran et al., 2018). The central layer is set to 1-m depth, trying to represent an irrigated land, and the dipoles are separated 5 m for a WUSN deployment. According to the results, as it is well known, the infinite dissipative model cannot be used when the quasi-static approximation is not guaranteed. Moreover, the free-space model is a good approximation for shallow burial depths.

The present simulation show that for WUSN, at very shallow depths, the frequency can be selected according to other design aspects than signal attenuation due to the medium. Taking into account that the induced voltage is increased by the frequency and also the available bandwidth and data rate, the key point for this application is to design efficient inductors with low resistivity for maximizing the coils coupling.

5.2. Underwater Communications

Among underwater communications, undersea sensing is a relevant application. Among the employed technologies, MI is being considered as it overcomes problems that face other technologies as highly environment dependent channel behavior in acoustic communications. This application involves data transmission from sea water into air and into sea water. MI channel path loss has been considered for different authors with different approaches (Akyildiz et al., 2015; Domingo, 2014; Wang et al., 2014; Wang et al., 2015).

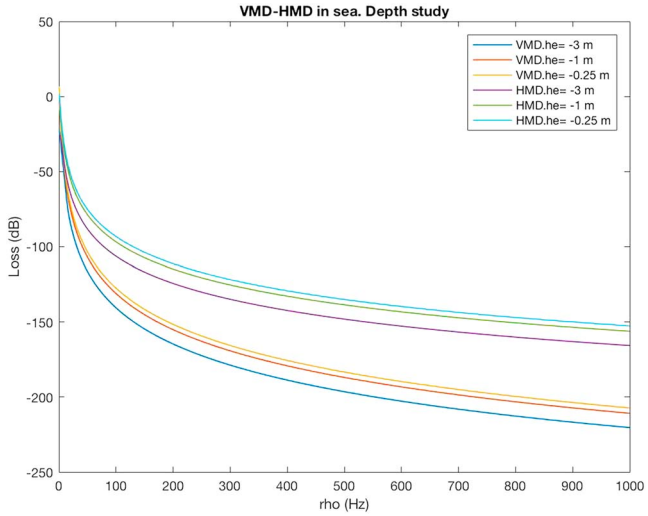

Figure 6. Absolute magnetic field for vertical magnetic dipole (VMD) and horizontal magnetic dipole (HMD) sources buried in seawater.

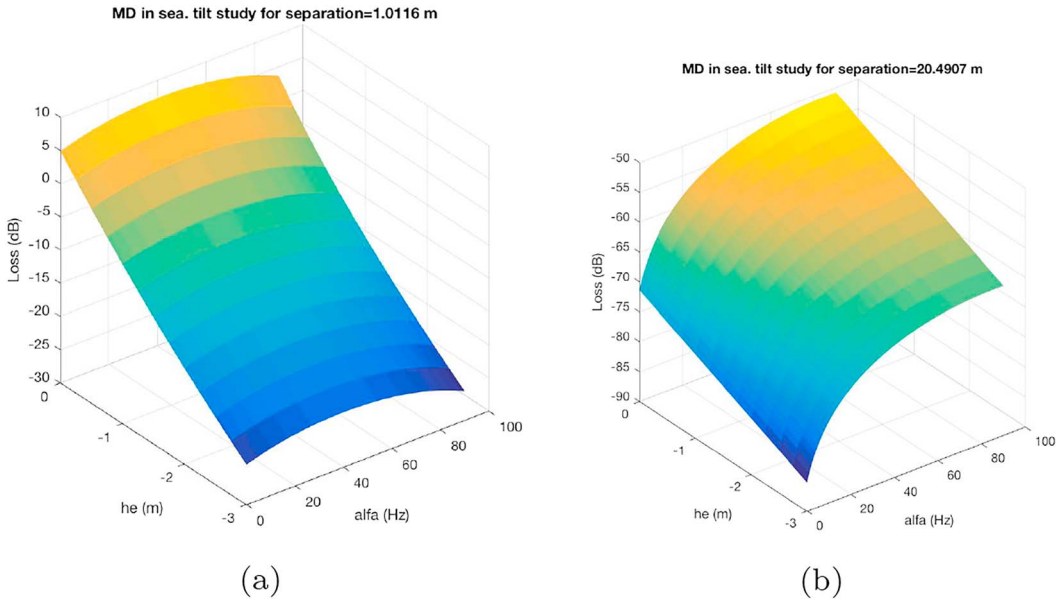

Figure 7. Magnetic dipole (MD) buried in seawater. Receiver at $z = 1.5$ m. Burial depth and dipole inclination effects. (a) Horizontal distance of 1 m. (b) Horizontal distance of 1 m.

The works by Wang et al. (2014, 2015) consider undersea to air communications with a three-layered model. Their formulation includes only their case of interest. Despite that their solutions and employed numerical method are different, our simulation results agree with those presented in their papers.

Now, we consider the effect of the source inclination for three different depths in order to analyze its influence together with the radial distance. Simulation parameters are set according to Wang et al. (2014). Figures 5 and 6 show the absolute magnetic field strength due to a VMD and a HMD source. As expected, the field due to the VMD is remarkably lower than that due to the HMD.

In addition, we analyze the source tilt effect, being $\alpha = 0$ for the VMD and $\alpha = 90^o$ for the HMD for horizontal distances of 1 and 20 m, see Figures 7 and 8, respectively. It can be observed that when the horizontal distance is low, the source tilt effects are not relevant. Moreover, for long distances, the horizontal dipole increases the received field significantly.

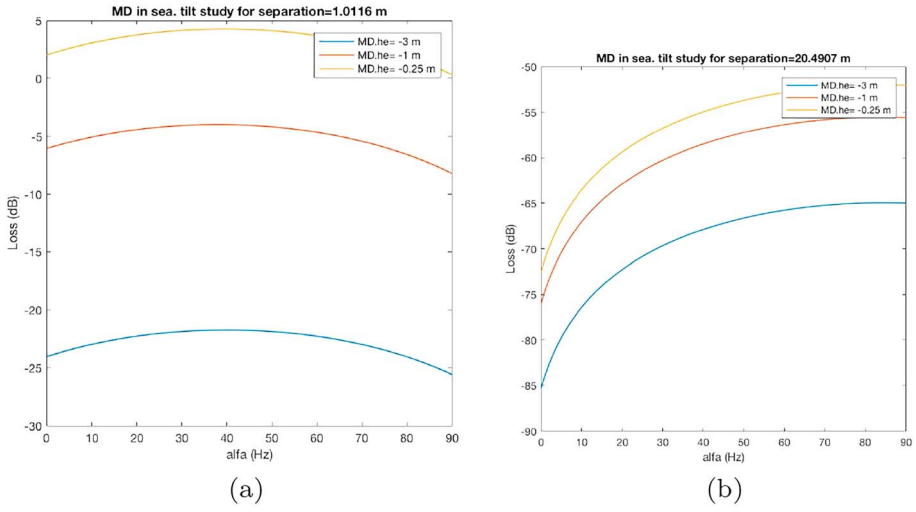

Figure 8. Magnetic dipole (MD) buried in seawater. Receiver at $z = 1.5$ m. Burial depth and dipole inclination effects. (a) Horizontal distance of 1 m. (b) Horizontal distance of 1 m.

6. Conclusion

In the present work, closed-form expressions for the magnetic fields of a magnetic dipole source (VMD and HMD) valid from the near zone to the far zone have been derived for horizontally stratified three-layered media in a comprehensive manner. They can be coded in an appropriate software for its evaluation or used directly from the implemented MATLAB code.

Moreover, as the formulation relies in Sommerfeld integrals, numerical integration is required. An integration algorithm has been derived for the highly accurate computations of the field expressions with low execution times.

The present numerical results have been validated using FEM models by the NRMSE fit metric. The measured differences among both numerical methods were approximately 1 for the VMD and 0.9 for the HMD case when there were no truncation effects for all the possible source-observer combinations for the electrical parameters and geometry limits considered.

Finally, two cases of study concerning WUSNs applications has been presented to show the usefulness of the proposed channel model and computational implementation.

Consequently, the numerical analysis of the present formulation has been proven as a reliable method for studying common subsurface problems with a desktop computer.

Acronyms

DOF	Degrees of freedom
EM	Electromagnetic
FEM	Finite Element Method
HMD	Horizontal magnetic dipole
MI	Magnetic induction
NRMSE	Normalized root-mean-square error
VMD	Vertical magnetic dipole
WUSNs	Wireless underground sensor networks

Acknowledgments
The authors would like to thank Llanwyn Jones for his kind help at the early beginnings of this work. They are also grateful to the I3A for making the most intensive computer simulations possible. This work has been supported by the Spanish MINECO Project Robot navigation and deployment in challenging environments—Robochallenge (ref. DPI2016-76676-RAEI/FEDER-UE). The financial support of the Aragon Government DGA T45-17R is also acknowledged. MATLAB functions for computational VMD and HMD field expressions, MATLAB scripts and data for the plots in this article can be found at https://github.com/nayuso/MI_Subsurface_Channel.

References

Abdu, H., Robinson, D. A., & Jones, S. B. (2007). Comparing bulk soil electrical conductivity determination using the DUALEM-1S and EM38-DD electromagnetic induction instruments. *Soil Science Society of America Journal*, *71*(1), 189–196.

Abo-Seida, O. (2002). Electromagnetic fields of thin circular loop antenna of arbitrary radius. *Cannadian Journal of Physics*, *80*, 29–37.

Abrudan, T. E., Kypris, O., Trigoni, N., & Markham, A. (2016). Impact of rocks and minerals on underground magneto-inductive communication and location. *IEEE Access*, *4*, 3999–4010.

Akyildiz, I. F., & Stuntebeck, E. P. (2006a). Wireless underground sensor networks: Research challenges. *Ad Hoc Networks*, *4*(6), 669–686.

Akyildiz, I. F., & Stuntebeck, E. P. (2006b). Wireless underground sensor networks: Research challenges. *Ad Hoc Networks*, *4*, 669–686.

Akyildiz, I. F., Wang, P., & Sun, Z. (2015). Realizing underwater communication through magnetic induction. *IEEE Communication Magazine*, *53*, 42–48.

Ayuso, N. (2010). Modeling and applications of through-the-earth magnetic field propagation (Ph.D. thesis), University of Zaragoza.

Ayuso, N., Cuchí, J. A., Lera, F., & Villarroel, J. L. (2006). Through-the-earth magnetic field propagation: Modelling and experimental validation, *Proceedings of the Antennas and Propagation Society International Symposium* (pp. 680–683). Albuquerque, NM, USA: IEEE.

Ayuso, N., Cuchí, J. A., Lera, F., & Villarroel, J. L. (2010). Accurately locating a vertical magnetic dipole buried in a conducting earth. *IEEE Transactions on Geoscience and Remote Sensing*, *48*(10), 3676–3685. https://doi.org/10.1109/TGRS.2010.2048918

Ayuso, N., Cuchí, J. A., Muñoz, A., Lera, F., & Villarroel, J. L. (2009). Through-the-earth magnetic field propagation: Modelling for underground applications, *Proceedings of the international conference on electromagnetics in advanced applications* (pp. 525–528). Torino, Italy: IEEE.

Ayuso, N., & Lera, F. (2019). Magnetic dipole field expressions and integration strategy for subsurface applications. http://webdiis.unizar.es/nayuso/MATLAB

Bandyiopadhyay, L., Chaulya, S., & Mishra, P. (2010). Wireless communication in underground mines, *RFID-Based Sensor Networking* (pp. 73–90). US: Springer.

Bannister, P. R. (1981). Image theory EM fields of horizontal dipole antennas in presence of conducting half-space (*NUSC Technical Report 6511*). New London, Connecticut: Naval Underwater Systems Center.

Becker, A., Elchert, D. C., & White, G. B. (1992). Measurement of sea ice conductivity by electromagnetic induction, *Proceedings OCEANS '92. Mastering the Oceans Through Technology* (Vol. 2, pp. 748–752). Newport, RI, USA, USA: IEEE. https://doi.org/10.1109/OCEANS.1992.607677

Burke, C. P., & Jones, D. L. (1994). Radio propagation in deep and shallow sea water (Tech. Rep. RP940101). London, U.K: Physics Department, King's College.

Chew, W. C., Jin, J.-M., Michielssen, E., & Song, J. (2001). *Fast and efficient algorithms in computational electromagnetics, Artech House, Inc.*Norwood, MA: COMSOL.

COMSOL Inc.: COMSOL Multiphysics - The Platform for Physics-Based Modeling and Simulation. Retrieved from http://www.comsol.com/comsol-multiphysics

Corwin, D. L., & Lesch, S. M. (2003). Application of soil electrical conductivity to precision agriculture: theory, principles, and guidelines. *Agronomy journal*, *95*(3), 455–471.
Davis, C. P., Chew, W. C., Tucker, W. W., & Atkins, P. R. (2008). A null-field method for estimating underground position. *IEEE Transactions on Geoscience and Remote Sensing*, *46*(11), 3731–3738. https://doi.org/10.1109/TGRS.2008.2000878
Domingo, M. C. (2014). Magnetic induction for underwater wireless communication networks. *Transactions on Antennas and Propagation*, *60*(6), 2929–2939.
Dong, X., & Vuran, M. C. (2011). A channel model for wireless underground sensor networks using lateral waves. In *IEEE Globecom*. Kathmandu, Nepa.
Durkin, J. (1983). Study of through-the-earth communications (PhD thesis), University of Pittsburgh.
Durkin, J. (1991). Earth conductivity estimates from through-the-earth electromagnetic transmission tests. *Transactions on geoscience and remote sensing*, *29*(2), 300–307.
Fei, T., Li, L. W., Yeo, T. S., Wang, H. L., & Wu, Q. (2007). A comparative study of radio wave propagation over the earth due to a vertical electric dipole. *IEEE Transactions on Antennas and Propagation*, *55*(10), 2723–2732. https://doi.org/10.1109/TAP.2007.905869
Fraser-Smith, A., & Bubenik, D. (1976). ULF/ELF magnetic fields generated at the sea surface by submerged magnetic dipoles. *Radio Science*, *11*(11), 901–913.
Gander, W., & Gautschi, W. (2000). Adaptive quadrature—Revisited. *BIT*, *40*(1), 84–101.
Guzatov, D., & Klimov, V. V. (2014). Focusing of dipole radiation by a negative index chiral layer. 2. A thin layer as compared with the wavelength. *Quantum Electronics*, *44*(12), 1112–11,148.
Guzatov, D., Klimov, V. V., & Poprukailo, N. S. (2013). Spontaneous radiation of a chiral molecule located near a half-space of a bi-isotropic material. *Journal of Experimental and Theoretical Physics*, *116*(4), 532–540.
Heil, K., & Schmidhalter, U. (2017). The application of EM38: Determination of soil parameters, selection of soil sampling points and use in agriculture and archaeology. *Sensors*, *17*(2540), 1–44.
Hochman, A., & Leviatan, Y. (2010). A numerical methodology for efficient evaluation of 2D Sommerfeld integrals in the dielectric half-space problem. *IEEE Transactions on Antennas and Propagation*, *58*(2), 413–431.
Inan, A., & Fraser-Smith, A. (1990). Further investigation of the interference minimum in the low-frequency electromagnetic fields produced by a submerged vertical magnetic dipole. *Radio Science*, *25*(4), 339–347.
Large, D., Ball, Laurence, & Farstad, A. (1973). Radio transmission to and from underground coal mines- theory and measurements. *IEEE Transactions on Communications*, *21*(3), 194–202.
Layman, G. E. (1981). Magnetic field strength below a horizontal magnetic dipole located at the earth or ocean surface. *Radio Science*, *16*(5), 871–876.
Liao, D., & Sarabandi, K. (2007). Modeling and simulation of near-earth propagation in presence of a truncated vegetation layer. *IEEE Transactions on Antennas and Propagation*, *55*(3), 949–957.
Lin, S.-C., Akyildiz, I. F., Wang, P., & Sun, Z. (2015). Distributed cross-layer protocol design for magnetic induction communication in wireless underground sensor networks. *IEEE Transactions on Wireless Communication*, *14*(7), 4006–4019.
Liu, L., & Li, K. (2007). Radiation from a vertical electric dipole in the presence of a three-layered region. *IEEE Transactions on Antennas and Propagation*, *55*(12), 3469–3475.
Long, Y., Jiang, H., & Rembold, B. (2001). Far-region electromagnetic radiation with a vertical magnetic dipole in sea. *IEEE Transactions on Antennas and Propagation*, *49*(6), 992–996.
Markham, A., Trigoni, N., Macdonald, D. W., & Ellwood, S. A. (2012). Underground localization in 3-D using magneto-inductive tracking. *IEEE Sensors Journal*, *12*(6), 1809–1816.
Michalski, K., & Mosig, J. (2016). The Sommerfeld half-space problem revisited: From radio frequencies and Zenneck waves to visible light and Fano modes. *Journal of Electromagnetic Waves and Applications*, *30*(2), 1–42.
Raj Mittra, P. P., & Rahmat-Samii, Y. (1979). Solving the current element problem over lossy half-space without Sommerfeld integrals. *IEEE Transactions on Antennas and Propagation*, *AP-27*(6), 778–782.
Shampine, L. (2008). Vectorized adaptive quadrature in MATLAB. *Journal of Computational and Applied Mathematics*, *211*, 131–140.
Shope, S. M. (1983). Above-the-earth field contours for a dipole buried in a homogeneous half-space (*Report of Investigations 8781*). Pittsburgh, PA: United States Bureau of Mines.
Silva, A. R., & Moghaddam, M. (2015). Operating frequency selection for low-power magnetic induction-based wireless underground sensor networks. In *IEEE Sensors Applications Symposium*. Zadar, Croatia.
Sinha, A., & Bhattacharya, P. K. (1966). Vertical magnetic dipole buried inside a homogeneous earth. *Radio Science*, *1*(3), 379–395.
Sogade, J., Vichabian, Y., Vandiver, A., Reppert, P. M., Coles, D., & Morgan, F. D. (2004). Electromagnetic cave-to-surface mapping system. *IEEE Transactions on Geoscience and Remote Sensing*, *42*(4), 754–763. https://doi.org/10.1109/TGRS.2003.819882
Sommerfeld, A. (1909). Über die Ausbreitung der Wellen in der drahtlosen Telegraphie. *Annals of Physics*, *28*, 665–737.
Sommerfeld, A. (1926). Über die Ausbreitung der Wellen in der drahtlosen Telegraphie. *Annals of Physics*, *81*, 1135–1153.
Stratton, J. (1941). *Electromagnetic theory*. N.Y. and London: McGraw-Hill.
Sun, Z., & Akyildiz, I. F. (2010). Magnetic induction communications for wireless underground sensor networks. *Transactions on Antennas and Propagation*, *58*(7), 2426–2435.
Sun, Z., & Akyildiz, I. F. (2012). On capacity of magnetic induction-based wireless underground sensor networks, *IEEE Infocom* (pp. 370–378). Orlando, USA: IEEE.
Tan, X., Sun, Z., & Akyildiz, I. F. (2015). Wireless underground sensor networks. MI-based communication systems for underground applications. *IEEE Antennas and Propagation Magazine*, *57*, 74–87.
Vuran, M. C., & Akyildiz, I. F. (2010). Channel model and analysis for wireless underground sensor networks in soil medium. *Physical Communication*, *3*, 245–254.
Vuran, M. C., Salam, A., Wong, R., & Irmak, S. (2018). Internet of underground things in precision agriculture: Architecture and technology aspects. *Ad Hoc Networks*, *81*, 160–173.
Wait, J. R. (1961). The electromagnetic fields of a horizontal dipole in the presence of a conducting half-space. *Canadian Journal of physics*, *39*, 1017–1028.
Wait, J. R. (1969). Electromagnetic fields of sources in lossy media. In R. E. Collin, & F. J. Zucker (Eds.), *Antenna Theory* (pp. 438–514). New York: McGraw-Hill. Part 2, Ch. 24.
Wait, J. R. (1972). Locating an oscillating magnetic dipole in the earth. *Electronics Letters*, *8*(16), 404–406.
Wait, J. R. (1982). *Geo-electromagnetism*. London: Academic Press.
Wait, J. R. (1996). Electromagnetic waves in stratified media, *IEEE/OUP series on electromagnetic wave theory* (pp. 438–514). New York: IEEE Press in assoc. with Oxford University Press.

Wait, J. R., & Spies, K. P. (1971). Subsurface electromagnetic fields of a line source on a conducting half-space. *Radio Science*, *6*(8,9), 781–786.
Wait, J. R., & Spies, K. P. (1972). Subsurface electromagnetic fields of a circular loop of current located above ground. *IEEE Transactions on Antennas and Propagation*, *20*, 520–522.
Wang, H., Yang, K., & Zheng, K. (2015). Electromagnetic field radiated in air from a horizontal/vertical magnetic dipole in sea. *Journal of Electromagnetic Waves and Applications*, *29*(7), 858–873.
Wang, H., Zheng, K., Yang, K., & Ma, Y. (2014). Electromagnetic field in air produced by a horizontal magnetic dipole immersed in sea: Theoretical analysis and experimental results. *IEEE Transactions on Antennas and Propagation*, *62*(9), 4647–4655. https://doi.org/10.1109/TAP.2014.2330600
Wei, Y., Holter, B., Simonsen, I., & Kuhnle, J. (2011). Calculations of Sommerfeld integrals for conductive media at low frequencies. In *International Conference on Electromagnetics*, Taipei, Taiwan.
Yan, L., Waynert, J., & Sunderman, C. (2013b). Measurements and modeling of through-the-earth communications for coal mines. *IEEE Transactions on Industry Applications*, *49*(5), 1979–1983.
Yan, L., Waynet, J. A., & Sunderman, C. (2013a). Measurements and modeling of through-the-earth communication for coal mines. *IEEE Transactions on Industry Applications*, *49*(5), 1979–1983.